Available online at www.synsint.com

Synthesis and Sintering

**ISSN** 2564-0186 (Print), **ISSN** 2564-0194 (Online)

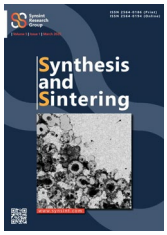

*Research article*

# Effect of calcination atmosphere and $Fe^{3+}$ content on $NiFe_xAl_{2-x}O_4$ nano pigments synthesized via a polyacrylamide gel method

**Rayehe Tavakolipour** [a,*], **Amir Abbas Nourbakhsh** [b,*]

[a] *Department of Materials Engineering, Naghshejahan Institute of Higher Education, Baharestan, Isfahan, Iran*
[b] *Department of Materials Science and Engineering, Shahreza Branch, Islamic Azad University, Shahreza, Iran*

ABSTRACT

In this research, $NiFe_xAl_{2-x}O_4$ pigments (x=0, 0.3, 0.7, and 1.5) were synthesized using a polyacrylamide gel method, and the effects of calcination atmosphere and the dopant amount on the formed phases and optical properties were investigated. The obtained pigments' physical, optical, and microstructural properties were clarified using the XRD, UV-Vis spectroscopy, and FESEM techniques. The phase analysis showed that the nickel carbide was formed in the reducing atmosphere instead of the spinel phase. So, the rest of the samples were prepared in an oxidizing atmosphere. The pigments that were obtained had a spherical morphology and a narrow particle size distribution due to the growth inhibitor role of the polyacrylamide network. The iron ions entered both tetrahedral and octahedral sites of the nickel aluminate structure, acted as the main chromophore, and turned the color from cyan to brown. Further addition of iron led to the darkening of the brown color.



KEYWORDS

Nickel aluminate
Spinel pigments
Polyacrylamide
Doping
Calcination atmosphere

OPEN ACCESS

## 1. Introduction

Spinel nano-pigments are a sub-class of inorganic colorants, consisting of nanoparticles with a general formula of $AB_2O_4$ ($A^{2+}$, $B^{3+}$, $O^{2-}$) which benefit from both unique properties of spinel structures and Nanomaterials, including high staining capacity, high abrasion resistance, high chemical/thermal stability, opacity, high color strength, as well as a uniform coverage [1]. The distribution of cations between octahedral and tetrahedral spaces determines the semiconductivity, coloring, catalytic, and magnetic properties of the spinels. Cationic distribution in the spinels can be described as $(A_{1-x}B_x)t[A_xB_{2-x}]_oO_4$, where x, t, and o indicate the inversion degree, tetrahedral, and octahedral spaces, respectively. The inversion degree (x) equals zero, ⅔, or 1 for normal, random, or inverse spinels, respectively. The inversion degree is generally a function of calcination temperature [2]. Transition metal oxide spinels are widely applied in the pigment industry due to their high chemical inertness and thermal stability [3]. These are two crucial factors for the pigments, especially for those meant to be applied in the glazes.

Aluminates are a high-temperature resistant group of spinel pigments with $AlO^{2-}$ as their oxyanion group [4]. Nickel aluminate ($NiAl_2O_4$) is a partially inverse transition metal oxide with a random distribution of $Ni^{2+}$ and $Al^{3+}$ ions in tetrahedral and octahedral spaces [5]. Nickel aluminate pigments have been synthesized using various methods, including solid-state [6, 7], sono-chemical [8] microwave irradiation [9], Pechini [10, 11], coprecipitation [11–13], mechano-chemical [14], gas-phase pyrolysis [15], hydrothermal [16], self-propagating high-temperature synthesis (SHS) [17–19], -based synthesis, sol-gel [20–22], immersion [23], microemulsion [24], and many more from pure, natural [4, 25] or waste [26, 27] resource. Although the solid-state method is suitable for the mass production of oxide powders, it has some major drawbacks, such as limited chemical homogeneity, large

* Corresponding authors. *E-mail address:* Rayehe.tavakolipour1990@gmail.com (R. Tavakolipour), Anourbakhs@yahoo.com (A.A. Nourbakhsh)
Received 26 February 2024; Received in revised form 27 March 2025; Accepted 28 March 2025.

https://doi.org/10.53063/synsint.2025.51208

particle size, high reaction temperature, low sinterability, and the possibility of impurity introductions [28]. Douy and Odier [28] introduced the polyacrylamide gel method for the preparation of mineral powders, which is simply based on a "solution-gel-calcination" process, benefiting from the acrylamide polymerization. The polyacrylamide gel grows into a network consisting of branches and interlocked ring-like cells where the precursor solution is separated, reducing the probability of powder agglomeration and providing small nano-powders with fewer agglomerates [29].

Various metals have been doped into the structure of nickel aluminate particles, mostly to enhance their catalytic [30–32] or electrochemical properties [33–35]. The coloring properties of nickel aluminate have been less explored compared to other aluminates, which could be due to its temperature-dependent cationic distributions [2], significantly affecting its optical properties. Gilabert et al. [36] synthesized (Ni, Co) (Cr, $Al)_2O_4$ pigments, and the results showed a wide color pallet from greens to deep blues with high stability in glazes; however, increasing the concentrations of dopants decreased the crystallinity. Elakkiya et al. [5] prepared copper-doped nickel aluminate pigments and stated that with only a small amount of dopant (0.02 mol), an environmentally friendly green pigment could be obtained. Gingasu et al. [37] observed a shift between inverse and normal spinel structures in the Ni-Co aluminate nano pigments with various amounts of cobalt and nickel cations. The latter increased the inversion degree.

As spinels are oxides, an oxidizing atmosphere has always been chosen for the synthesis, but the behavior of a combination of salts and acrylamide monomers in a reducing atmosphere has not been investigated yet. In this study, the synthesis of $NiFe_xAl_{2-x}O_4$ pigments was attempted in both reducing and oxidizing atmospheres to evaluate the functionality of the polyacrylamide gel method for the synthesis of spinels in various conditions. Also, the effect of $Fe^{3+}$ on the formed phases, cationic occupancy, and coloring properties of the pigments were clarified.

## 2. Materials and methods

### *2.1. Materials*

Applied materials in this project, including nickel nitrate hexahydrate ($Ni(NO_3)_2.6H_2O$) (nickel source), aluminum nitrate nonahydrate ($Al(NO_3)_3.9H_2O$) (aluminum source), iron(III) nitrate nonahydrate ($Fe(NO_3)_3.9H_2O$) (dopant source), acrylamide (monomer), N,N'-methylenebisacrylamide (crosslinker), ammonium persulfate (catalyst) and tetramethylethylenediamine (accelerator) were all purchased from Merck and used without any further purifications.

### *2.2. Pigment synthesis*

Molar ratios of materials were selected and weighted according to Table 1. Nitrate salts were added to 50 cc distilled water in a beaker on a magnetic stirrer at 50 °C. After a clear solution was obtained, acrylamide and methylenebisacrylamide were added to the solution with a ratio of 20:1. After the solution was completely homogenized, ammonium persulfate (0.33 g) and tetra tetramethylethylenediamine (0.3 cc) were added to the aqueous solution of salts and monomers. The gelation process was initiated immediately after the catalyst additions, and the solution turned into a transparent and flexible gel. The gel was dried at 150 °C for 3 h. Then, the dried gel was calcined at 1000 °C for 2 h in oxidizing or reducing (Ar) atmospheres. The calcination temperature was selected according to the previous studies [8], which showed that a complete crystallization of nickel aluminate required a temperature above 950 °C. A simplified scheme of the synthesis process is shown in Fig. 1.

### *2.3. Characterization*

X-ray diffraction technique (X'Pert, Model TW3714, Philips Company) was used to investigate the crystallinity and estimate the crystallite sizes of the calcined samples using a CuKα in 2θ=0 °–85 ° with a step of 0.02 ° at 40 KV and 30 mA. A UV-Vis spectrophotometer (JASCO V-670) in a wavelength range of 190–900 nm was applied to evaluate the optical properties (color) of the samples containing various amounts of dopant, which were calcined in an oxidizing atmosphere. Microstructural observations were conducted using a field-emission scanning electron microscopy technique (Model JSM 6400, JOEL Company).

## 3. Results and discussion

### *3.1. X-ray diffraction*

As the presence of more than 30% iron interrupts the X-ray Diffraction analysis and decreases the accuracy, only FTN1 and FTN1-R with a medium iron amount (0.3 mol) were picked among the iron-containing samples. Fig. 2 shows the XRD patterns of the samples calcined in the reducing atmosphere. As seen in Fig. 2a, all peaks of the undoped sample (TN1-R) corresponded well with JCPDS card No. 014-0020,

**Table 1.** Compositions and calcination conditions used for the synthesis of $NiFe_xAl_{2-x}O_4$ pigments.

| Sample code | Calcination conditions | | | Concentration | | Molar ratios (mole/mole) | | |
|---|---|---|---|---|---|---|---|---|
| | Atmosphere | | Temperature (°C) | Salts | Monomers | Ni | Al | Fe |
| | Reducing | Oxidizing | | | | | | |
| TN1-R | + | - | 1000 | 0.5 | 1.5 | 1.0 | 2.0 | 0 |
| FTN1-R | + | - | 1000 | 0.5 | 1.5 | 1.0 | 1.7 | 0.3 |
| TN1 | - | + | 1000 | 0.5 | 1.5 | 1.0 | 2.0 | 0 |
| FTN1 | - | + | 1000 | 0.5 | 1.5 | 1.0 | 1.7 | 0.3 |
| FTN2 | - | + | 1000 | 0.5 | 1.5 | 1.0 | 1.3 | 0.7 |
| FTN3 | - | + | 1000 | 0.5 | 1.5 | 1.0 | 0.5 | 1.5 |

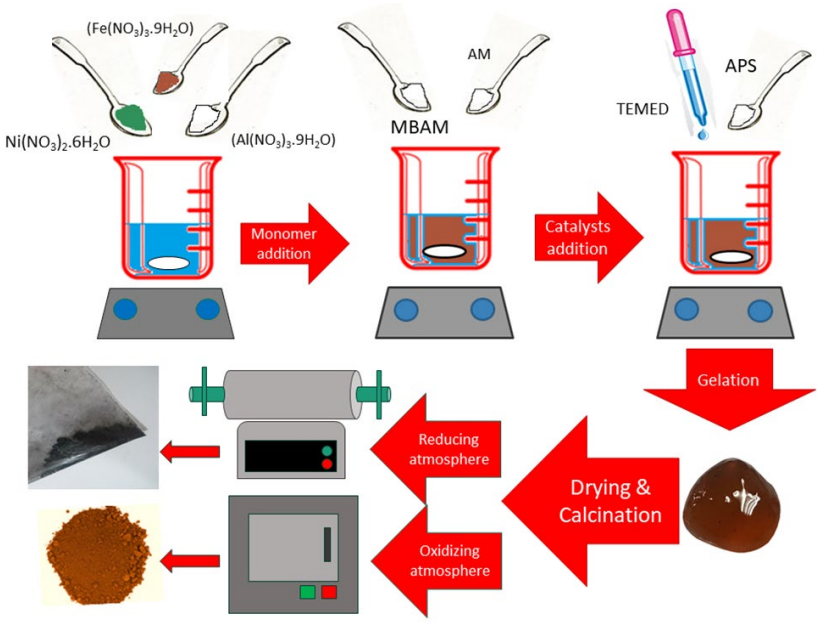


**Fig. 1.** A simplified scheme of the synthesis of samples using the polyacrylamide gel method in various calcination atmospheres. (AM: acrylamide, MBAM: N,N'-methylenebisacrylamide, APS: ammonium persulfate, and TEMED: tetramethylethylenediamine).

confirming the formation of Nickel carbide in the sample. The reason could be explained in this way: When the temperature was raised to 450 °C, the released CO gas from the polymers reduced the nickel oxide and reacted with the metallic Ni and formed NiC. This was confirmed by the Ellingham diagram where CO and NiO plots intersected at 450 °C (Fig. 3). Also, a large amount of nickel was observed in the XRD patterns of both doped and undoped samples in the reducing atmosphere, confirming the above statement. Aluminum oxide remained unreacted in the sample as $Al_2O_3$, NiO, and CO had no intercepts below 2000 °C (Fig. 3). The lack of a characteristic peak for $Al_2O_3$ could be due to its ultra-small size. The large amount of carbon in the final compositions was from the acrylamide network, which could not find a chance to exit from the samples. The iron-doped sample (FTN1-R) had a similar pattern with more intense NiC peaks (Fig. 2b). No spinel formation was due to the lack of oxygen. So, synthesis in the reducing atmosphere was discontinued, and the rest of the study was followed on the samples calcined in an oxidizing atmosphere.

Fig. 4 shows the XRD patterns of the samples calcined in an oxidizing atmosphere (TN1 and FTN1). As seen, about 90% of the peaks in the XRD pattern of TN1 (Fig. 4a) correspond well with JCPDS card no. 10-339, confirming the formation of nickel aluminate ($NiAl_2O_4$) with a fully crystalline structure. $NiAl_2O_4$ peaks were located at 2θ of 22.182 °, 36.637 °, 43.254 °, 52.765 °, 66.040 °, 70.572 °, and 77.882 °, corresponding well with (111), (220), (311), (400), (422), (511), and (440) planes. Two small peaks at 50.732 ° and 74.547 ° belonged with NiO, which showed a little remanent nickel oxide in the structure. The characteristic peaks of the iron-doped nickel aluminate (FTN1) shifted to smaller diffraction angles. Nickel oxide was not detected in this sample.

The mean crystallite sizes of samples TN1 and FTN1 were calculated using the Scherrer formula:

$$L = \frac{0.98\lambda}{\beta \cos\theta} \quad (1)$$

where L, λ, β, and θ are crystallite size (nm), X-ray wavelength (0.154 nm), full width at half maximum (rad), and the diffraction angle, respectively. Table 2 shows the calculated crystallite sizes of TN1 and FTN1 samples. As seen, the difference between the mean crystallite sizes of doped and undoped samples was negligible.

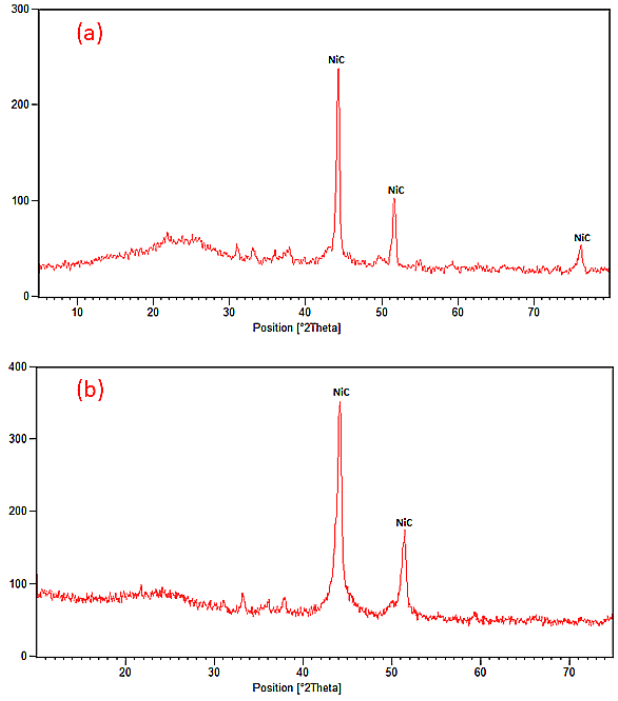


**Fig. 2.** XRD patterns of a) pure TN1 and b) iron-doped samples (FTN1-R) in a reducing atmosphere.

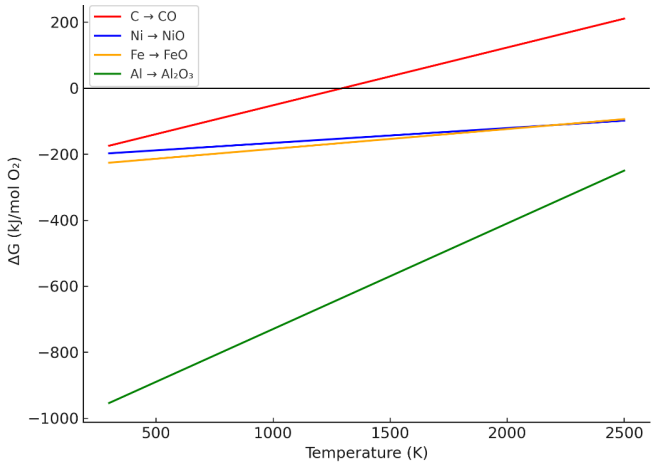


**Fig. 3.** Ellingham diagram of CO, NiO, FeO, and $Al_2O_3$.

### *3.2. Microstructural observations*

Fig. 5 shows the FESEM image of the sample FTN1. As seen, all particles were spherical, and most of them had a uniform size, ranging between 23–27 nm. Few agglomerates were seen, which could be due to the tendency of ultra-small particles towards agglomeration. However, most of the particles showed no significant desire for growing and sintering after the removal of the organic network, confirming the suitability of the polyacrylamide gel method for the synthesis of nanopowders. Interestingly, the particle sizes corresponded well to the estimated crystallite sizes from XRD patterns, indicating the single-crystallite particles.

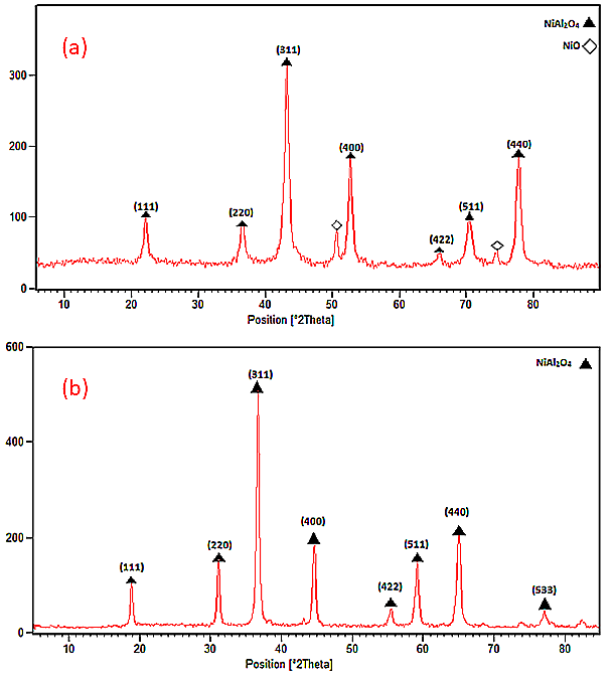


**Fig. 4.** XRD patterns of $NiFe_xAl_{2-x}O_4$ pigments: a) pure TN1 and b) iron-doped samples (FTN1) in an oxidizing atmosphere.

### *3.3. UV-Vis spectroscopy*

Fig. 6 shows diffuse spectra of all samples synthesized in an oxidizing atmosphere with various amounts of iron (0, 0.3, 0.7, and 1.5). The undoped sample (TN1) showed three bands at about 362 nm, 609 nm, and 710 nm, with a shoulder at 516 nm. According to the previous studies [8], the band at 609 nm was attributed to the octahedral nickel and the rest to the octahedral one. The main reflectance of sample TN1 in the visible region was seen at 490–520 nm, belonging to the cyan color. As seen, iron addition diminished the bands at 300 nm and 600 nm. Only a band was seen at 700 nm (related to the octahedral nickel), belonging to the longest wavelength in the visible region, i.e., the brown color. The reason could be explored in the inverse spinel structure of the nickel ferrite ($NiFe_2O_4$) structure. In the nickel ferrite, iron is distributed in both tetrahedral and octahedral spaces, while nickel is only located in the tetrahedral ones [38]. It seemed that when iron ions were introduced to the random spinel structure of nickel aluminate, they reproduced the same manner in the presence of nickel. So, they occupied both octahedral and tetrahedral spaces and acted as the dominant chromophore, shifting the color from cyan to brown. Also, it appeared that the substitution of $Al^{3+}$ smaller ions with large $Fe^{3+}$ resulted in a lattice distortion. Increasing the amount of iron dopant decreased the total reflectance percentage, indicating a color darkening.

**Table 2.** Mean crystallite size of undoped and doped pigments.

| Sample code | Mean crystallite size (nm) |
|---|---|
| TN1 | 23.1 |
| FTN1 | 23.8 |

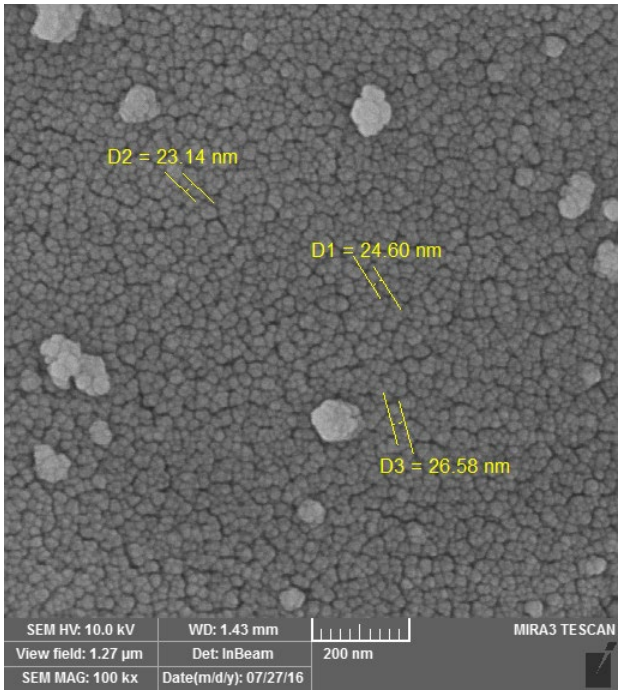


**Fig. 5.** FESEM image of $NiFe_xAl_{2-x}O_4$ (FTN1) nano pigments calcined in an oxidizing atmosphere.

## 4. Conclusions

In this project, it was attempted to synthesize $NiFe_xAl_{2-x}O_4$ spinel nano pigments (x=0, 0.3, 0.7, and 1.5) using a polyacrylamide gel method and evaluate the formed phases in various (oxidizing and reducing) atmospheres. No spinel phase was obtained in the reducing atmosphere, as the lack of oxygen inhibited the removal of carbon from the thermally dissociated polyacrylamide network, leading to the formation of NiC with large amounts of remanent nickel and aluminum oxide in the structure. Nickel aluminate was successfully formed in the oxidizing atmosphere with a high purity. A narrow particle size distribution within the nanoscale and uniformly spherical morphology confirmed the efficiency of the polyacrylamide network in the particle growth inhibition and synthesis of nanoparticles with minimum agglomerates. The trivalent iron dopant significantly affected the optical properties of nickel aluminate pigments as it entered both octahedral and tetrahedral spaces, acted as the main chromophore, and changed the color from cyan to brown. Further iron additions led to a color darkening. No NiO was detected in the iron-doped samples, suggesting a purer composition in the doped samples.

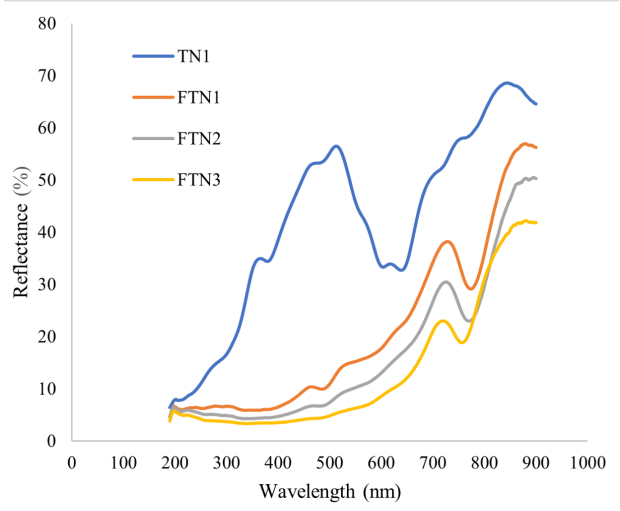


**Fig. 6.** DRS spectra of the synthesized $NiFe_xAl_{2-x}O_4$ pigments in an oxidizing atmosphere.

## CRediT authorship contribution statement

**Rayehe Tavakolipour:** Writing – original draft, Conceptualization, Project administration, Resources.
**Amir Abbas Nourbakhsh:** Writing – review & editing, Investigation, Supervision, Validation.

## Data availability

The data underlying this article will be shared on reasonable request to the corresponding author.

## Declaration of competing interest

The authors declare no competing interests.

## Funding and acknowledgment

This research received no external funding. The authors have no acknowledgments to declare.

## References

[1] R. Tavakolipour, R. Pournajaf, E. Grazenaite, Synthesis and doping of high-temperature resistant spinel nano pigments: A review, Synth. Sinter. 4 (2024) 17–28. https://doi.org/10.53063/synsint.2024.41191.
[2] Y.S. Han, J.B. Li, X.S. Ning, B. Chi, Temperature dependence of the cation distribution in nickel aluminate spinel from thermodynamics and X-rays, J. Am. Ceram. Soc. 88 (2005) 3455–3457. https://doi.org/10.1111/j.1551-2916.2005.00603.x.
[3] G.B. Kunde, G.D. Yadav, Green strategy for the synthesis of mesoporous, free-standing MAl2O4 (M = Fe, Co, Ni, Cu) spinel films by sol–gel method, Mater. Sci. Eng: B. 271 (2021) 115244. https://doi.org/10.1016/j.mseb.2021.115244.
[4] M. Dalpasquale, F.Q. Mariani, M. Müller, F.J. Anaissi, Citrus pectin as a template for synthesis of colorful aluminates, Dyes Pigments. 125 (2016) 124–131. https://doi.org/10.1016/j.dyepig.2015.10.015.
[5] V. Elakkiya, R. Abhishekram, S. Sumathi, Copper doped nickel aluminate: Synthesis, characterisation, optical and colour properties, Chin. J. Chem. Eng. 27 (2019) 2596–2605. https://doi.org/10.1016/j.cjche.2019.01.008.
[6] Y.S. Han, J.B. Li, X.S. Ning, B. Chi, Effect of preparation temperature on the lattice parameter of nickel aluminate spinel, J. Am. Ceram. Soc. 87 (2004) 1347–1349. https://doi.org/10.1111/j.1151-2916.2004.tb07733.x.
[7] Y.S. Han, J.B. Li, X.S. Ning, X.Z. Yang, B. Chi, Study on NiO excess in preparing NiAl2O4, Mater. Sci. Eng: A. 369 (2004) 241–244. https://doi.org/10.1016/j.msea.2003.11.026.

[8] P. Jeevanandam, Y. Koltypin, A. Gedanken, Preparation of nanosized nickel aluminate spinel by a sonochemical method, Mater. Sci. Eng: B. 90 (2002) 125–132. https://doi.org/10.1016/S0921-5107(01)00928-X.
[9] M.M. Amini, L. Torkian, Preparation of nickel aluminate spinel by microwave heating, Mat. Lett. 57 (2002) 639–642. https://doi.org/10.1016/S0167-577X(02)00845-5.
[10] L. Gama, M.A. Ribeiro, B.S. Barros, R.H.A. Kiminami, I.T. Weber, A.C.F.M. Costa, Synthesis and characterization of the NiAl2O4, CoAl2O4 and ZnAl2O4 spinels by the polymeric precursors method, J. Alloys Compd. 483 (2009) 453–455. https://doi.org/10.1016/j.jallcom.2008.08.111.
[11] M. Hasan, J. Drazin, S. Dey, R.H.R. Castro, Synthesis of stoichiometric nickel aluminate spinel nanoparticles, Am. Mineral. 100 (2015) 652–657. https://doi.org/10.2138/am-2015-4997.
[12] M. Gabrovska, D. Nikolova, M. Shopska, L. Bilyarska, R. Edreva-Kadjieva, et al., Ni–Al Layered Double Hydroxides as Precursors of Ceramic Pigments, Proceedings of the III Advanced Ceramics and Applications Conference, Atlantis Press, Paris. (2016) 205–220. https://doi.org/10.2991/978-94-6239-157-4_15.
[13] M. Gil-Calvo, C. Jiménez-González, B. de Rivas, J.I. Gutiérrez-Ortiz, R. López-Fonseca, Effect of Ni/Al molar ratio on the performance of substoichiometric NiAl2O4 spinel-based catalysts for partial oxidation of methane, Appl. Catal. B. 209 (2017) 128–138. https://doi.org/10.1016/j.apcatb.2017.02.063.
[14] M.K. Nazemi, S. Sheibani, F. Rashchi, V.M. Gonzalez-Delacruz, A. Caballero, Preparation of nanostructured nickel aluminate spinel powder from spent NiO/Al2O3 catalyst by mechano-chemical synthesis, Adv. Powder Technol. 23 (2012) 833–838. https://doi.org/10.1016/j.apt.2011.11.004.
[15] P. Hasin, N. Nattamon, R. Barni, A. Laobuthee, Nickel-aluminium complex: a simple and effective precursor for nickel aluminate (NiAl2O4) spinel, Maejo Int. J. Sci. Technol. 2 (2008) 140–149.
[16] M. Paul, N. Pal, A. Bhaumik, Mesoporous nickel-aluminum mixed oxide: A promising catalyst in hydride-transfer reactions, Eur. J. Inorg. Chem. (2010) 5129–5134. https://doi.org/10.1002/ejic.201000732.
[17] A. Tirsoaga, D. Visinescu, B. Jurca, A. Ianculescu, O. Carp, Eco-friendly combustion-based synthesis of metal aluminates MAl2O4 (M = Ni, Co), J. Nanoparticle Res. 13 (2011) 6397–6408. https://doi.org/10.1007/s11051-011-0392-1.
[18] N.M. Deraz, Synthesis and Characterization of Nano-Sized Nickel Aluminate Spinel Crystals, Int. J. Electrochem. Sci. 8 (2013) 5203–5212. https://doi.org/10.1016/S1452-3981(23)14674-8.
[19] S. Jayasree, A. Manikandan, S.A. Antony, A.M. Uduman Mohideen, C. Barathiraja, Magneto-Optical and Catalytic Properties of Recyclable Spinel NiAl 2O4 Nanostructures Using Facile Combustion Methods, J. Supercond. Nov. Magn. 29 (2016) 253–263. https://doi.org/10.1007/s10948-015-3249-5.
[20] N. Bayal, P. Jeevanandam, Synthesis of metal aluminate nanoparticles by sol-gel method and studies on their reactivity, J. Alloys Compd. 516 (2012) 27–32. https://doi.org/10.1016/j.jallcom.2011.11.080.
[21] M. Maddahfar, M. Ramezani, M. Sadeghi, A. Sobhani-Nasab, NiAl2O4 nanoparticles: synthesis and characterization through modify sol–gel method and its photocatalyst application, J. Mater. Sci: Mater. Electron. 26 (2015) 7745–7750. https://doi.org/10.1007/s10854-015-3419-z.
[22] M. Rahimi-Nasrabadi, F. Ahmadi, M. Eghbali-Arani, Different morphologies fabrication of NiAl2O4 nanostructures with the aid of new template and its photocatalyst application, J. Mater. Sci: Mater. Electron. 28 (2017) 2415–2420. https://doi.org/10.1007/s10854-016-5812-7.
[23] S. Komeili, A. Taeb, M. Takht Ravanchi, M. Rahimi Fard, The properties of nickel aluminate nanoparticles prepared by sol–gel and impregnation methods, Res. Chem. Intermed. 42 (2016) 7909–7921. https://doi.org/10.1007/s11164-016-2568-x.
[24] F. Meyer, R. Hempelmann, S. Mathur, M. Veith, Microemulsion mediated sol-gel synthesis of nano-scaled MAl2O4 (M = Co, Ni, Cu) spinels from single-source heterobimetallic alkoxide precursors, J. Mater. Chem. 9 (1999) 1755–1763. https://doi.org/10.1039/a900014c.
[25] C. Ragupathi, J.J. Vijaya, P. Surendhar, L.J. Kennedy, Comparative investigation of nickel aluminate (NiAl2O4) nano and microstructures for the structural, optical and catalytic properties, Polyhedron. 72 (2014) 1–7. https://doi.org/10.1016/j.poly.2014.01.013.
[26] K. Shih, J.O. Leckie, Nickel aluminate spinel formation during sintering of simulated Ni-laden sludge and kaolinite, J. Eur. Ceram. Soc. 27 (2007) 91–99. https://doi.org/10.1016/j.jeurceramsoc.2006.04.176.
[27] D.F.L. Horsth, J.O. Primo, M. Dalpasquale, C. Bittencourt, F.J. Anaissi, Colored aluminates pigments obtained from metallic aluminum waste, an opportunity in the circular economy, Clean. Eng. Technol. 5 (2021) 100313. https://doi.org/10.1016/j.clet.2021.100313.
[28] A. Douy, P. Odier, The polyacrylamide gel: A novel route to ceramic and glassy oxide powders, Mater. Res. Bull. 9 (1989) 1119–1126. https://doi.org/10.1016/0025-5408(89)90069-X.
[29] H. Wang, L. Gao, W. Li, Q. Li, Preparation of nanoscale α-Al2O3 powder by the polyacrylamide gel method, Nanostruct. Mater. 11 (1999) 1263–1267. https://doi.org/10.1016/S0965-9773(99)00417-1.
[30] A. Nair, A. Kurian, S. Sumathi, Photocatalytic degradation of organic pollutants using yttrium and copper co-doped nickel aluminate, Res. Sq. (2024). https://doi.org/10.21203/rs.3.rs-5295270/v1.
[31] E. Regulska, J. Breczko, A. Basa, A.T. Dubis, Rare-earth metals-doped nickel aluminate spinels for photocatalytic degradation of organic pollutants, Catalysts. 10 (2020) 1–13. https://doi.org/10.3390/catal10091003.
[32] P.S. Patil, R.S. Dhivare, S.R. Mirgane, B.G. Pawar, T.R. Mane, Cobalt-Doped Nickel Aluminate Nanomaterials Synthesis, Characterization, and Catalytic Properties, Macromol. Symp. 393 (2020) 2000163. https://doi.org/10.1002/masy.202000163.
[33] R. Vladoiu, A. Mandes, V. Dinca, E. Matei, S. Polosan, Synthesis of Cobalt–Nickel Aluminate Spinels Using the Laser-Induced Thermionic Vacuum Arc Method and Thermal Annealing Processes, Nanomaterials. 12 (2022) 3895. https://doi.org/10.3390/nano12213895.
[34] S. Srinivas, Y.S. Vidya, H.C. Manjunatha, Upendra, R. Munirathnam, et al., Photoluminescence and supercapacitor potential of eco-friendly synthesized NiAl2O4 nanoparticles, Ceram. Int. (2025). https://doi.org/10.1016/j.ceramint.2025.02.203.
[35] W. Tibermacine, M. Omari, Structural and electrochemical properties of Fe-doped NiAl2O4 oxides, J. Fundam. Appl. Sci. 11 (2019) 227–244.
[36] J. Gilabert, M.D. Palacios, V. Sanz, S. Mestre, Effects of composition and furnace temperature on (Ni, Co) (Cr, Al)2O4 pigments synthesized by solution combustion route, Int. J. Appl. Ceram. Technol. 15 (2018) 179–190. https://doi.org/10.1111/ijac.12761.
[37] D. Gingasu, O. Oprea, G. Marinescu, J.M. Calderon Moreno, D.C. Culita, et al., Structural, Morphological, and Optical Properties of Single and Mixed Ni-Co Aluminates Nanoparticles, Inorganics (Basel). 11 (2023) 371. https://doi.org/10.3390/inorganics11090371.
[38] A. Kale, S. Gubbala, R.D.K. Misra, Magnetic behavior of nanocrystalline nickel ferrite synthesized by the reverse micelle technique, J. Magn. Magn. Mater. 277 (2004) 350–358. https://doi.org/10.1016/j.jmmm.2003.11.015.